Discovery of Resolved Magnetically Split Lines in SDSS/APOGEE Spectra of 157 Ap/Bp Stars

S. Drew Chojnowski[1] , Swetlana Hubrig[2] , Sten Hasselquist[3], Fiorella Castelli[4], David G. Whelan[5] , Steven R. Majewski[6] , Christian Nitschelm[7], D. A. García-Hernández[8,9], Keivan G. Stassun[10] , and Olga Zamora[8,9]

[1] Apache Point Observatory and New Mexico State University, P.O. Box 59, Sunspot, NM 88349-0059, USA
[2] Leibniz-Institut für Astrophysik Potsdam (AIP), An der Sternwarte 16, D-14482 Potsdam, Germany
[3] Department of Physics & Astronomy, University of Utah, 115 1400 E, Salt Lake City, UT 84112, USA
[4] Istituto Nazionale di Astrofisica, Osservatorio Astronomico di Trieste, via Tiepolo 11, I-34143 Trieste, Italy
[5] Department of Physics, Austin College, 900 North Grand Avenue, Sherman, TX 75090, USA
[6] Department of Astronomy, University of Virginia, P.O. Box 400325, Charlottesville, VA 22904-4325, USA
[7] Centro de Astronomía (CITEVA), Universidad de Antofagasta, Avenidos Angamos 601, Antofagasta 1270300, Chile
[8] Instituto de Astrofísica de Canarias (IAC), E-38205 La Laguna, Tenerife, Spain
[9] Universidad de La Laguna (ULL), Departamento de Astrofísica, E-38206 La Laguna, Tenerife, Spain
[10] Department of Physics and Astronomy, Vanderbilt University, Nashville, TN 37235, USA

Abstract

We report on magnetic field measurements of 157 chemically peculiar A/B stars (Ap/Bp) based on resolved, magnetically split absorption lines present in H-band spectra provided by the Sloan Digital Sky Survey (SDSS)/ Apache Point Observatory Galactic Evolution Experiment (APOGEE) survey. These stars represent the extreme magnetic end of a still-growing sample of >900 Ap/Bp stars selected among the APOGEE telluric standard stars as those with Ce III absorption lines and/or literature Ap/Bp classifications. The lines most frequently resolved into their split components for these stars in the H-band pertain primarily pertain to Ce III, Cr II, Fe I, Mn II, Si I, and Ca II, in addition to one or more unidentified ions. Using mean magnetic field modulus ($\langle B \rangle$) estimates for transitions with known Landé factors, we estimate effective Landé factors for 5 Ce III lines and 15 unknown lines and proceed to measure $\langle B \rangle$ of 157 stars, only 3 of which have previous literature estimates of $\langle B \rangle$. This 183% increase in the number of Ap/Bp stars for which $\langle B \rangle$ has been measured is a result of the large number of stars observed by SDSS/APOGEE, extension of high-resolution Ap/Bp star observations to fainter magnitudes, and the advantages of long wavelengths for resolving magnetically split lines. With $\langle B \rangle \sim 25$ kG, the star 2MASS J02563098+4534239 is currently the most magnetic star of the SDSS/APOGEE sample. Effective Landé factors, representative line profiles, and magnetic field moduli are presented. The validity of the results is supported using optical, high-resolution, follow-up spectra for 29 of the stars.

Key words: atomic data – infrared: stars – stars: chemically peculiar – stars: magnetic field

Supporting material: machine-readable tables

1. Introduction

Globally ordered magnetic fields are observed in roughly 10%–20% of intermediate and massive main sequence stars with spectral types between approximately F0 and B2. These stars, generally called chemically peculiar Ap and Bp stars (referred to as Ap stars in the rest of this Letter, for simplicity's sake), exhibit strong overabundances of certain iron peak elements and rare earths. The majority also exhibit under-abundances of He, C, and O relative to solar abundances (e.g., Ghazaryan et al. 2018), though the more massive Bp stars usually show overabundances of He and Si (e.g., Castro et al. 2017). These effects are caused by the disruption of normal diffusion processes by the strong magnetic fields. As stars of more than a few solar masses are expected to lack significant surface convection zones in which magnetic dynamos are generated in low-mass stars, the strong magnetic fields of Ap stars are unexpected and often attributed to fossil fields inherited from the collapsed gas clouds (Moss 2001).

The magnetic fields of Ap stars are most frequently diagnosed through spectropolarimetric measurements of the mean longitudinal field, $\langle B_z \rangle$, which is strongly dependent on the line of sight but can be obtained for the majority of Ap stars regardless of their rotation rates. However, an important group is formed by the Ap stars with low projected rotational velocities and strong kG magnetic fields. For these stars, conventional spectroscopy of sufficient resolution can be used to measure the mean magnetic field modulus, $\langle B \rangle$, based on the wavelength separations of resolved, magnetically split lines (RMSLs). Although somewhat dependent on the geometry of the observation, $\langle B \rangle$ has the advantage of being primarily determined by the intrinsic stellar magnetic field strength. Prior to this work, 84 Ap stars with RMSLs were known (Mathys 2017), and their study allowed the measurement of their magnetic fields and the establishment of a number of general properties. The star with the strongest magnetic field currently known, "Babcock's Star" (HD 215441), is a B8V star with a surface dipole field strength of 34 kG (Babcock 1960; Preston 1969).

The vast majority of past studies of Ap stars with RSMLs have relied on optical data of very slowly rotating stars (for which the Doppler effect does not serve to blend the split components), but spectroscopy at longer wavelengths provides several advantages in terms of resolving magnetically split lines. For example, the wavelength separation of magnetically split components is proportional to the square of the wavelength, such that for the fixed effective Landé factor, the spectral resolution required to resolve the split components of a

line is significantly lower in the *H*-band than it would be in the optical. Further, the Doppler effect has a linear dependence on wavelength, such that magnetic splitting can be resolved in the *H*-band for stars that are rotating too fast for the splitting to be resolved in the optical.

In this Letter we present the analysis of a sub-sample of 154 new stars with RMSLs in the *H*-band, as well as of 3 stars for which RMSLs had been observed previously in the optical. The 157 stars were identified among the largest-ever spectroscopic survey of Ap stars to date, being carried out by the Sloan Digital Sky Survey (SDSS-III and SDSS-IV; Eisenstein et al. 2011; Blanton et al. 2017) sub-survey known as the Apache Point Observatory Galactic Evolution Experiment (APOGEE; Majewski et al. 2017). This near-tripling of the number of Ap stars with $\langle B \rangle$ measurement is due partially to the volume and depth of the APOGEE survey. The 157 RSML stars were identified among a much larger sample of $\sim$1000 Ap/Am stars with multi-epoch APOGEE observations, and the 91/157 stars with *V* magnitudes greater than 10 represents a 3000% increase in the number of $V > 10$ Ap stars for which $\langle B \rangle$ has been measured.

2. Data

2.1. APOGEE H-band Spectroscopy

This Letter focuses primarily on data from the two APOGEE instruments, which are 300-fiber, $R = 22,500$, *H*-band spectrographs that operate on the Sloan 2.5 m telescope (Gunn et al. 2006) at Apache Point Observatory (APO) and on the Du Pont 2.5 m telescope at Las Campanas Observatory. Throughout this Letter, we refer to vacuum wavelengths when discussing the *H*-band data. Each APOGEE instrument records most of the *H*-band (15145–16960 Å) on three detectors, with coverage gaps between 15800–15860 Å and 16430–16480 Å and with each fiber having a $\sim$2″ diameter on-sky field of view. Total exposure times in each observation are about one hour, and the the 2°–3° diameter APOGEE fields are usually observed multiple times on different nights, months, or years, to accumulate signal for fainter targets and to check for radial velocity variability. Individual spectra are ultimately combined into high signal-to-noise ratio (S/N) spectra for chemical abundance analysis. A detailed description of the APOGEE survey was presented by Majewski et al. (2017), and the data reduction process has been described in Nidever et al. (2015).

As discussed in Zasowski et al. (2013, 2017), 35/300 APOGEE fibers are placed on blank sky positions to facilitate the removal of airglow emission features from science spectra, and a further 15–35/300 fibers are placed on quasi-randomly selected hot stars that facilitate removal of telluric absorption features from science spectra. The latter are generally the bluest and brightest available stars in the field and are restricted to a magnitude range of roughly $6.5 < H < 11.0$. They are selected mostly based on raw Two Micron All-Sky Survey (2MASS; Skrutskie et al. 2006) $J - K$ color but also with spatial restrictions to account for variation of the telluric absorption across the field. To date, the APOGEE instruments have observed >40,000 telluric standard stars, permitting the serendipitous discovery of exotic objects including highly magnetized OB stars (Eikenberry et al. 2014), Be stars (Chojnowski et al. 2015), as well as a large sample of >900 Ap stars, some of which are the focus of this Letter.

2.2. ARCES Optical Spectroscopy

We also obtained optical spectra of 29 stars using the Astrophysical Research Consortium Echelle Spectrograph (ARCES; Wang et al. 2003) on the ARC 3.5 m telescope at APO. ARCES covers the full optical spectrum (3500–10000 Å) at a resolution of $R = 31,500$. We used standard Image Reduction and Analysis Facility (IRAF[11]) echelle data reduction techniques, including 2D to 1D extraction, bias subtraction, scattered light and cosmic ray removal, flat-field correction, wavelength calibration via Thorium–Argon lamp exposures, as well as continuum normalization and merging of orders.

3. Sample Selection

The APOGEE Ap star sample currently consists of 986 stars that APOGEE has observed together more than 5500 times, with the about 85% of the stars having been identified among the APOGEE telluric standard stars via an algorithm designed to search for the presence of the doubly ionized Cerium (Ce III) lines that are usually the strongest absorption features aside from the broad hydrogen Bracket series lines. The other 15% of the stars lack the Ce III lines and were instead added to the sample based on literature Ap/Bp/Am classifications (for detailed definitions of these spectral classes, see Chapter 5.2 of Gray & Corbally 2009). These 986 Ap/Bp/Am stars therefore account for just over 2% of the APOGEE telluric standard stars, but this should be taken as a lower limit to the true fraction.

Whereas the overall sample will be discussed in future work, this Letter deals with the 157 stars (886 total spectra) for which RMSLs were visually identified in one or more APOGEE spectra. For the majority of the 157 stars, RMSLs appear in multiple observations such that absorption lines in the combined spectra clearly exhibit splitting. However, 17/157 stars have only been observed once to date, and in another 49/157 cases, the RMSLs were noticed and measured in an individual spectrum rather than the combined spectrum. Usually this was due to one of the individual spectra having significantly higher S/N than the others, but in some cases, it was almost certainly due to temporal variability of the magnetic field strength.

4. Line Identification

We used the APOGEE linelist (Shetrone et al. 2015) to identify the majority of absorption lines present in the *H*-band spectra. Atomic data for the Ce III lines was obtained from a Ce III linelist computed by Biémont et al. (2002). This linelist was previously used by Hubrig et al. (2012; provided to them as private communication by Biemont et al.), who were the first to confirm the presence of Ce III lines in *H*-band spectra of Ap stars. For the optical follow-up spectra, we relied on the Kurucz linelist[12] for line identification.

One or more ions are clearly missing from our *H*-band linelist, as indicated by several unidentified lines exhibiting RMSLs in the spectra of numerous stars. These features are
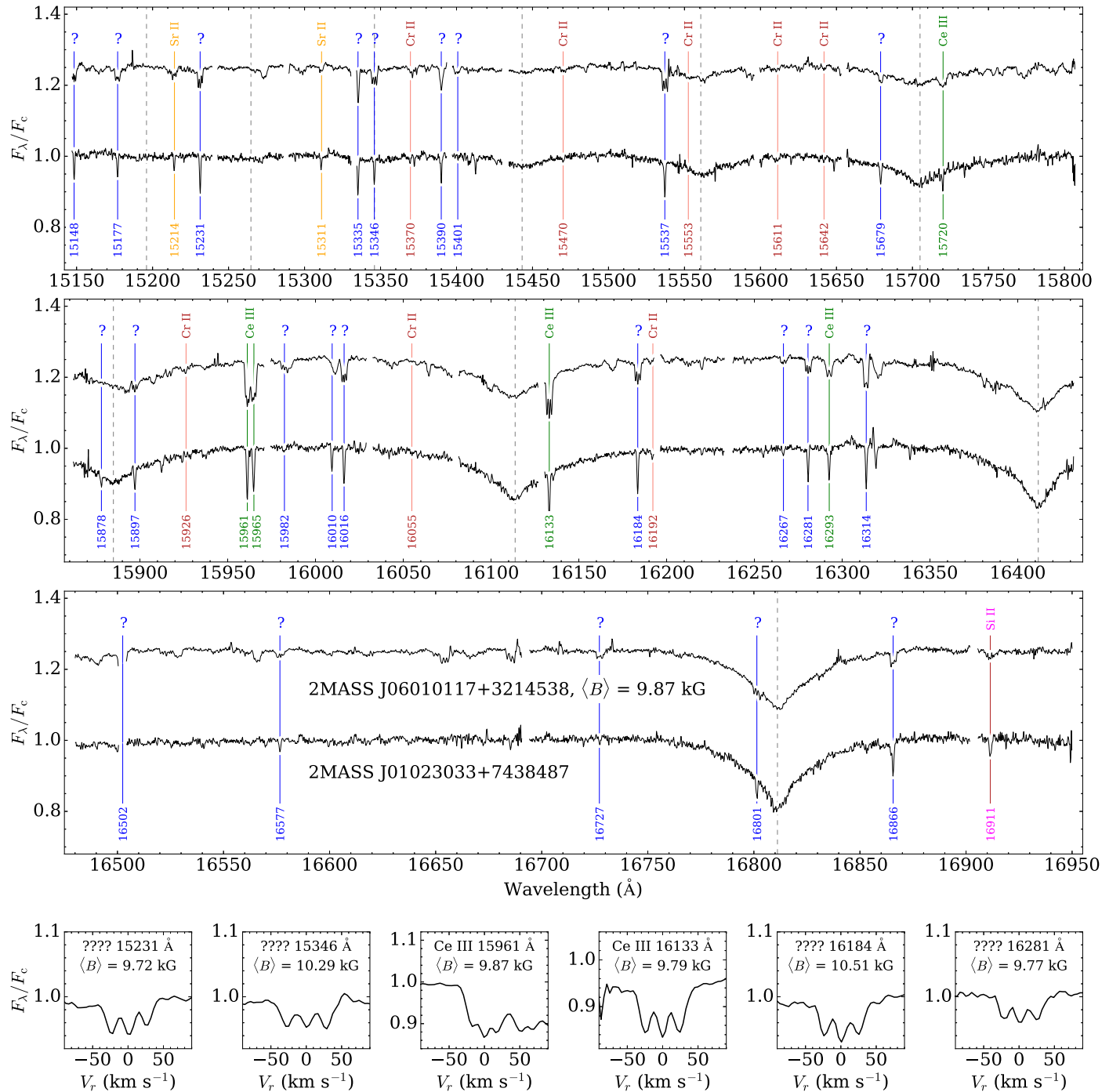

Figure 1. Top three rows: APOGEE spectra of 2MASS J06010117+3214538 and 2MASS J01023033+7438487, two stars exhibiting the unknown lines discussed in Section 4, with the lines being magnetically split for the former. Blue vertical lines indicate the unknown lines (for which the labels are the vacuum rest wavelengths in Å) and green lines indicate Ce III. A few other species in common between the two stars are labeled. Strong airglow lines have been masked from the spectra, including one that typically distorts the profile of the unknown line at 16502 Å. Bottom row: a closer view of magnetically split lines in the spectrum of 2MASS J06010117+3214538. The feature redward of Ce III 15961 Å is a blend of Si I 15964 Å and Ce III 15965 Å. The mean magnetic field modulus obtained from the measured splitting of each line is given.

usually detected simultaneously and they are occasionally the only metallic absorption features beyond Ce III. They are probably due to some heavy element that cannot be identified owing to the limited availability of atomic data for $\lambda > 10000$ Å. The strongest of these unknown lines is the 16184 Å line, for which magnetically split components are observed in ∼31% of the larger Ap star sample. We used a sub-sample of 20 narrow-lined Ap stars exhibiting the unknown

lines to measure accurate wavelengths for the features. Figure 1 displays the full APOGEE spectrum of one such narrow-lined star (2MASS J01023033+7438487) along with a star for which the unknown lines are magnetically split (2MASS J06010117 +3214538).

The Ce III lines (15961, 15965, 16133 Å, and in cases of strong Ce III, also 16292 and 15720 Å) are present in 100% of the sample at hand, with the 16133 Å line exhibiting RMSLs

Table 1
Effective Landé g Factors

Ion	λ_{vac} (Å)	log(gf)	J_{low}	g_{low}	E_{low} (eV)	J_{high}	g_{high}	E_{high} (eV)	g_{eff}	N_{stars}
C I	16009.273	−0.090	2.0	1.000	9.631	3.0	1.001	10.406	1.002 ± 0.050	3
C I	16026.078	−0.140	2.0	1.000	9.631	3.0	1.074	10.405	1.148 ± 0.050	6
C I	16895.031	0.568	2.0	1.000	9.003	3.0	0.978	9.736	0.956 ± 0.050	19
Mg I	15753.291	−0.060	1.0	1.501	5.932	2.0	1.167	6.719	1.000 ± 0.050	2
Mg I	15770.150	0.380	2.0	1.501	5.933	3.0	1.334	6.719	1.167 ± 0.050	8
Mg II	16764.796	0.480	0.5	0.666	12.083	1.5	0.800	12.822	0.834 ± 0.050	9
Mg II	16804.520	0.730	1.5	1.334	12.085	2.5	1.200	12.822	1.099 ± 0.050	8
Al I	16723.524	0.152	0.5	0.666	4.085	1.5	0.800	4.827	0.834 ± 0.050	6
Al I	16755.140	0.408	1.5	1.334	4.087	2.5	1.200	4.827	1.099 ± 0.050	10
Si I	15888.794	−0.740	1.0	0.508	5.954	1.0	1.472	6.734	0.990 ± 0.050	2

(This table is available in its entirety in machine-readable form.)

for 63% of the sample and with the weaker 15961 Å and 16292 Å lines being split for 43% and 32% of the sample, respectively. The Ce III 15965 Å line is often blended with the strongest Si I line covered (15964 Å), such that the splitting of Ce III 15965 Å can only be measured when the presence of Si I lines can be ruled out by confirming absence of Si I 15893 Å and 16685 Å. The fraction of stars with Ce III 16133 Å measurements would be even higher were it not for a strong airglow feature (16129 Å) that is often poorly subtracted and may coincide with the blue wing of the Ce III line depending on the stellar radial velocity.

Cr II is the next most frequently magnetically split ion, with the splitting of the 15370 and 15470 Å lines being measurable in 50% and 39% of the sample, respectively. Other particularly useful lines include Fe I 15299 Å (34%), Fe I 15626 Å (31%), Fe I 16491 Å (27%), Si I 16685 Å (25%), as well as the unidentified line at 16184 Å (31%). Unlike the situation in the optical, where Ap stars typically exhibit numerous Fe II and Ti II lines, no Fe II lines are confidently detected in the spectra of any stars, and Ti II detections are quite rare. The star 2MASS J23102121+4717017 is the only available example where more than two magnetically split Ti II lines were resolved.

5. Mean Magnetic Field Modulus Measurement

Given the measurements of the wavelength separations of magnetically split components in a given absorption line and knowledge of the Landé g factors of the associated energy levels, it is straightforward to compute the mean magnetic field modulus $\langle B \rangle$ in units of Gauss according to

$$\langle B \rangle = \frac{\Delta\lambda}{k\, g_{\text{eff}}\, \lambda_0^2}. \qquad (1)$$

Here, $\Delta\lambda$ is the separation in Å between an outer and the central split component or else half of the separation between outer components in a triplet profile. λ_0 is the rest wavelength of the line in Å and k is a constant, 4.67×10^{-13} Å^{-1} G^{-1}. It is important to note that although we have only analyzed spectral lines exhibiting apparent triplet profiles like those shown in the lower panels of Figure 1, the Zeeman patterns (see Mathys 1990) of the H-band lines have not been investigated and Equation (1) is therefore an approximation.

The effective Landé factor (g_{eff}) of a given transition is calculated using the total angular momentum quantum numbers (J) and Landé factors (g) of the lower (1) and upper level (2) as follows:

$$g_{\text{eff}} = \frac{1}{2}(g_1 + g_2) + \frac{1}{4}(g_1 - g_2)[J_1(J_1 + 1) - J_2(J_2 + 1)], \qquad (2)$$

where in the case of $J_1 = J_2$, g_{eff} is simply the average of the Landé factors of the lower and upper levels.

To measure $\Delta\lambda$, we either fit Gaussians to the absorption features or simply estimated their positions visually. This was done interactively using the *splot* program in IRAF. For each star, the splitting was measured for as many lines as possible and the results were averaged, with assumed or derived errors on g_{eff} being propagated appropriately. On average, measurements from ∼13 lines per star were used, but the range of number of lines used is quite large. In a few cases, the magnetic splitting could only be measured in two to three lines, often because the only metallic lines present are Ce III. In the case of 2MASS J06365367+0118455 however, the splitting of 61 lines was measured.

The J and g values used here were taken from the Kurucz linelist, and we assumed a constant uncertainty of 0.02 for the g_{eff} of lines with existing laboratory data. However, laboratory data are unavailable for the Ce III lines and for the unknown lines (see Section 4), such that it was necessary to estimate the g_{eff} of these lines. To do so, we defined a sub-sample of 34/157 stars with high-S/N spectra, particularly well-resolved magnetically split features, and measurements of lines with known g_{eff} in addition to Ce III and the unknown lines. The lines with known g_{eff} were used to calculate preliminary $\langle B \rangle$ measurements for the 34 stars. These values were then used derive average estimates of g_{eff} for the Ce III and unknown lines.

Table 1 summarizes the 149 lines used for measurement of $\langle B \rangle$, providing the vacuum wavelength, log(gf), energy levels, and g_{eff} for each line, as well as the number of stars for which magnetic splitting was measured. Overall, we find relatively low g_{eff} for Ce III and the unknown lines, which together average $g_{\text{eff}} \sim 1.07$. The weak Ce III 15720 Å line has the highest estimated value at $g_{\text{eff}} \sim 1.39$, but unfortunately this line is rarely observed.
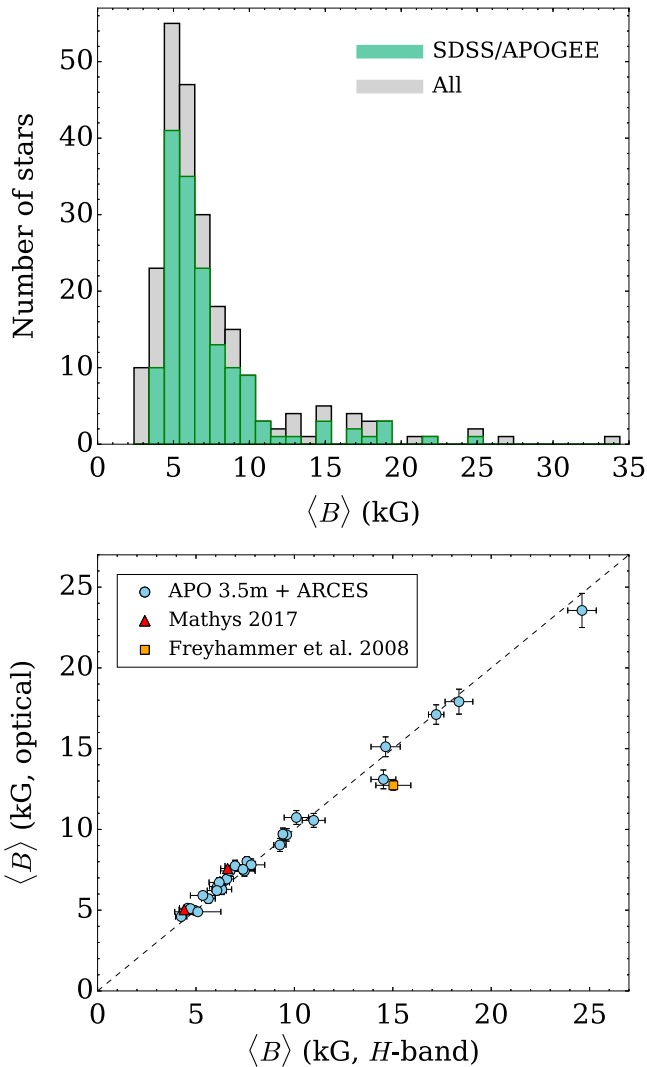
Figure 2. Upper panel: histogram of the magnetic field modulus for all 238 Ap stars with resolved, magnetically split lines. The new additions from SDSS/ APOGEE are shaded in green. Lower panel: comparison of $\langle B \rangle$ as measured in the H-band vs. the optical. The dashed line indicates perfect agreement.

5.1. H-band Results

The upper panel of Figure 2 shows the distribution of measured $\langle B \rangle$ of all Ap stars known to exhibit RMSLs, with the new discoveries presented in this Letter shaded in green and with those from Mathys (2017) shaded in gray. The average for the APOGEE sample is $\langle B \rangle \sim 7.1$ kG, while the average for all stars including those of Mathys (2017) is a bit higher at $\langle B \rangle \sim 7.3$ kG due to the inclusion of Babcock's Star. The distribution of $\langle B \rangle$ measured using APOGEE spectra ranges from ~ 3.6 kG in the case of 2MASS J02463240+0001145 up to ~ 25 kG in the case of 2MASS J02563098+4534239. A total of 19 new examples of stars with $\langle B \rangle > 10$ kG are identified, thus filling in the previous gap between 10–11 kG.

The lower limit on $\langle B \rangle$ of ~ 3.5 kG measurable from the APOGEE spectra is a consequence of resolving power, whereby the smallest splitting that we can measure is about 0.6 Å. For a star with strong Mn I 15222 Å ($g_{\mathrm{eff}} = 1.969$), splitting should be visible down to $\langle B \rangle$ of just below 3 kG. No such examples have been found, however, meaning that it is not possible to investigate the notion of an intrinsic lower limit to measurable field strength of $\langle B \rangle \sim 2$ kG (Mathys 2017).

Figure 3 shows an example of a magnetically split line for each of the 157 stars, generally showing the most clearly resolved line. In the cases where Ce III 16133 Å is displayed, narrow spikes blueward of the line are residuals from the imperfect removal of the aforementioned strong airglow line at 16129 Å.

5.2. Optical Results

The same procedure described in Section 5 was applied to the 29 optical follow-up spectra obtained with the ARC 3.5 m telescope and ARCES spectrograph in order to provide a sanity check on the H-band measurements of $\langle B \rangle$. As expected, the stars exhibit numerous RMSLs in the optical. For the 19/29 stars with $\langle B \rangle < 8$ kG, we relied primarily on limited numbers of long wavelength lines (7000–10200 Å), while for the 10/29 stars with $\langle B \rangle > 9$ kG, we measured hundreds of RMSLs for each star, keeping the 50 lines nearest to the average. Another 3 of the 157 stars were included in the Mathys (2017) sample of stars for which magnetically split lines had been previously resolved in optical spectra.

As demonstrated in the lower panel of Figure 2, we find good agreement overall between the H-band and optical measurements, with the results agreeing to within a kG in most cases. The most discrepant results pertain to the star 2MASSJ 07123042-2103537 (HD 55540), where we find $\langle B \rangle = 15.0$ kG despite Freyhammer et al. (2008) having found $\langle B \rangle = 12.7$ kG. The three available APOGEE spectra of this star allow us to confirm that not only is the difference due to temporal variability of the observed $\langle B \rangle$, but also that the star is indeed radial velocity variable as pointed out by Freyhammer et al. (2008).

We also used the optical spectra to estimate traditional spectral types based on comparison of the target stars to a sample of 30 bright A and B stars with spectra in the ELODIE Archive (Prugniel & Soubiran 2001). Stars with clear detections of He I 4471 Å and weak or missing Fe I, Mg I, Ca I, and Mn I lines were assigned temperature classes of B8 or B9, while the A stars were classified based on the equivalent widths of temperature-dependent lines (e.g., Fe I 4045 Å, Mg I 5183 Å, Ca I 4227 Å, Mn I 4031 Å) as well the ratios of neutral versus singly ionized lines (e.g., Mg I/Mg II and Fe I/Fe II). Due in part to difficulty finding the continuum around the wings of the hydrogen Balmer series lines in the ARCES camera's small wavelength ranges per order, luminosity classes were not estimated. Anomalously strong absorption lines from Si, Cr, Sr, and Eu are specifically flagged.

Table 2 summarizes the H-band and optical magnetic field modulus measurements, giving 2MASS designations, alternate identifiers, V magnitudes from UCAC4 (Zacharias et al. 2013), H magnitudes from 2MASS, the number of APOGEE spectra of each star, the S/N of the combined spectrum, a literature or estimated spectral type if available, the magnetic field modulus $\langle B \rangle$, and the number of spectral lines used to measure $\langle B \rangle$. In the cases where optical measurements were available, the final columns of Table 2 provide the associated $\langle B \rangle$ measurement and the number of spectral lines used. Less reliable measurements of $\langle B \rangle$, usually due to large scatter between different lines and/or measurements near the resolution limit of APOGEE are given in parentheses in Table 2.
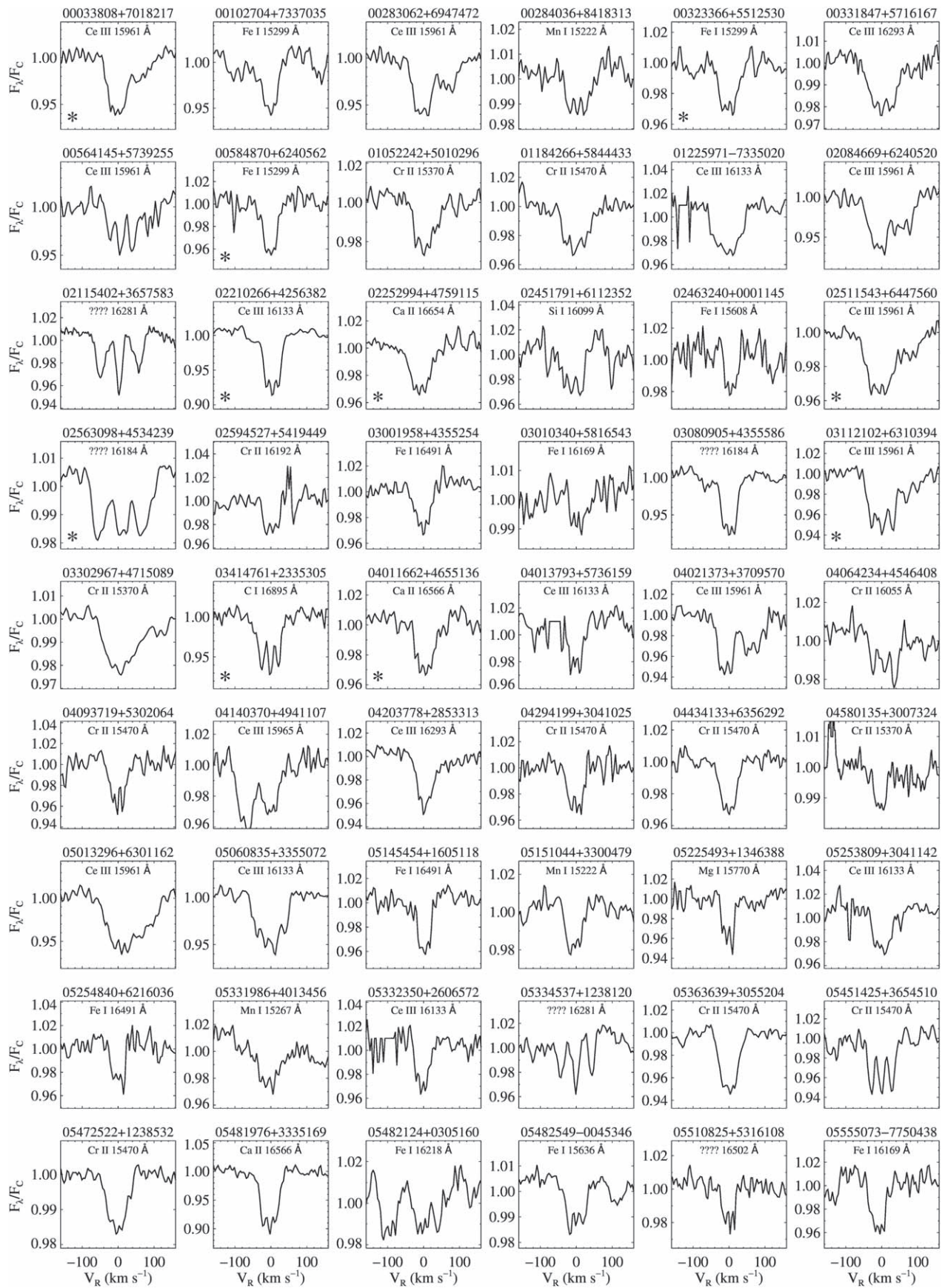
Figure 3. Montage of Zeeman split lines in the SDSS/APOGEE spectra for all 157 stars. 2MASS designations are provided above each panel, and asterisks in the lower-left corners of some panels indicate that the presence of resolved, magnetically split lines was confirmed via higher-resolution optical spectra.
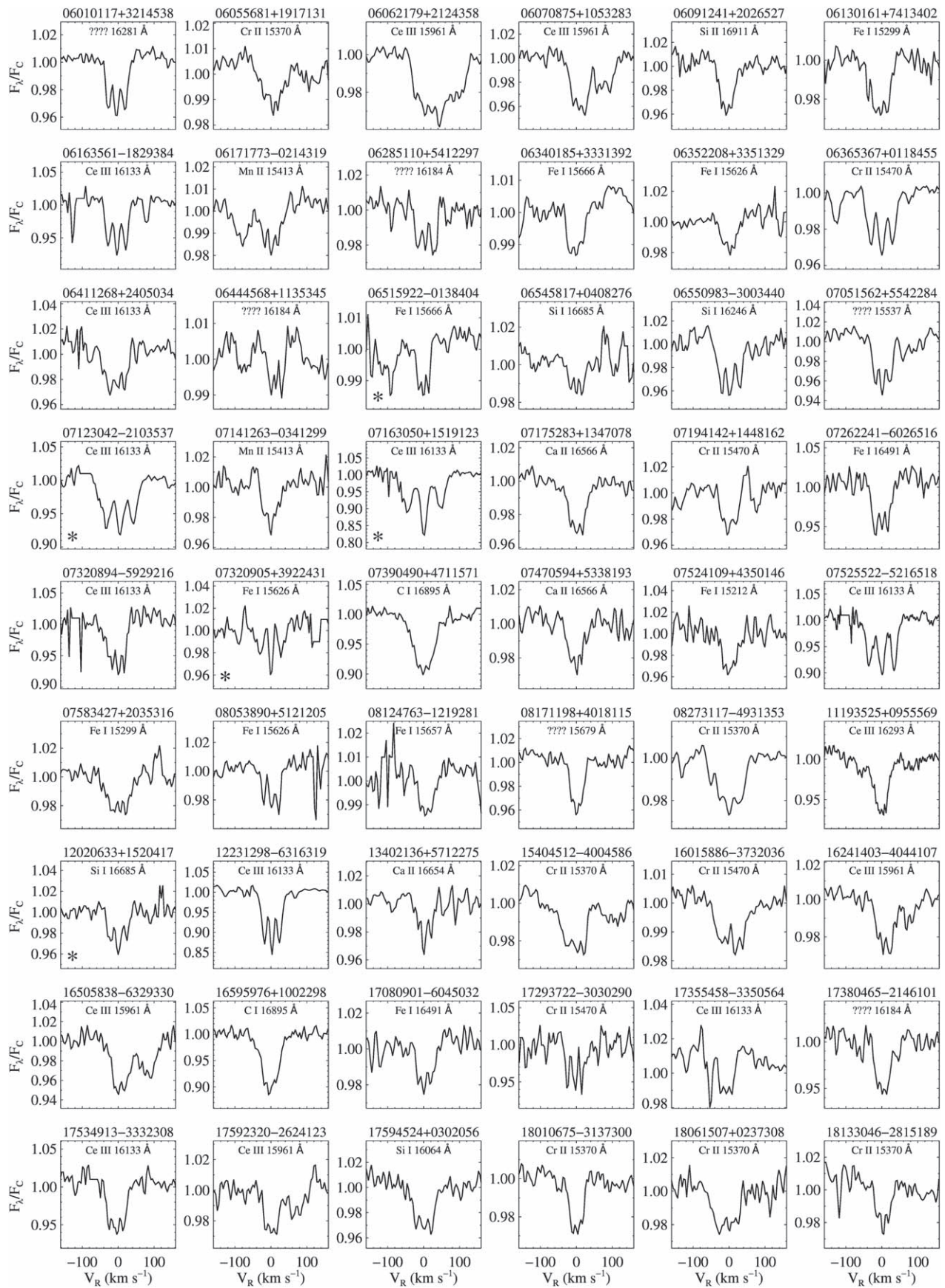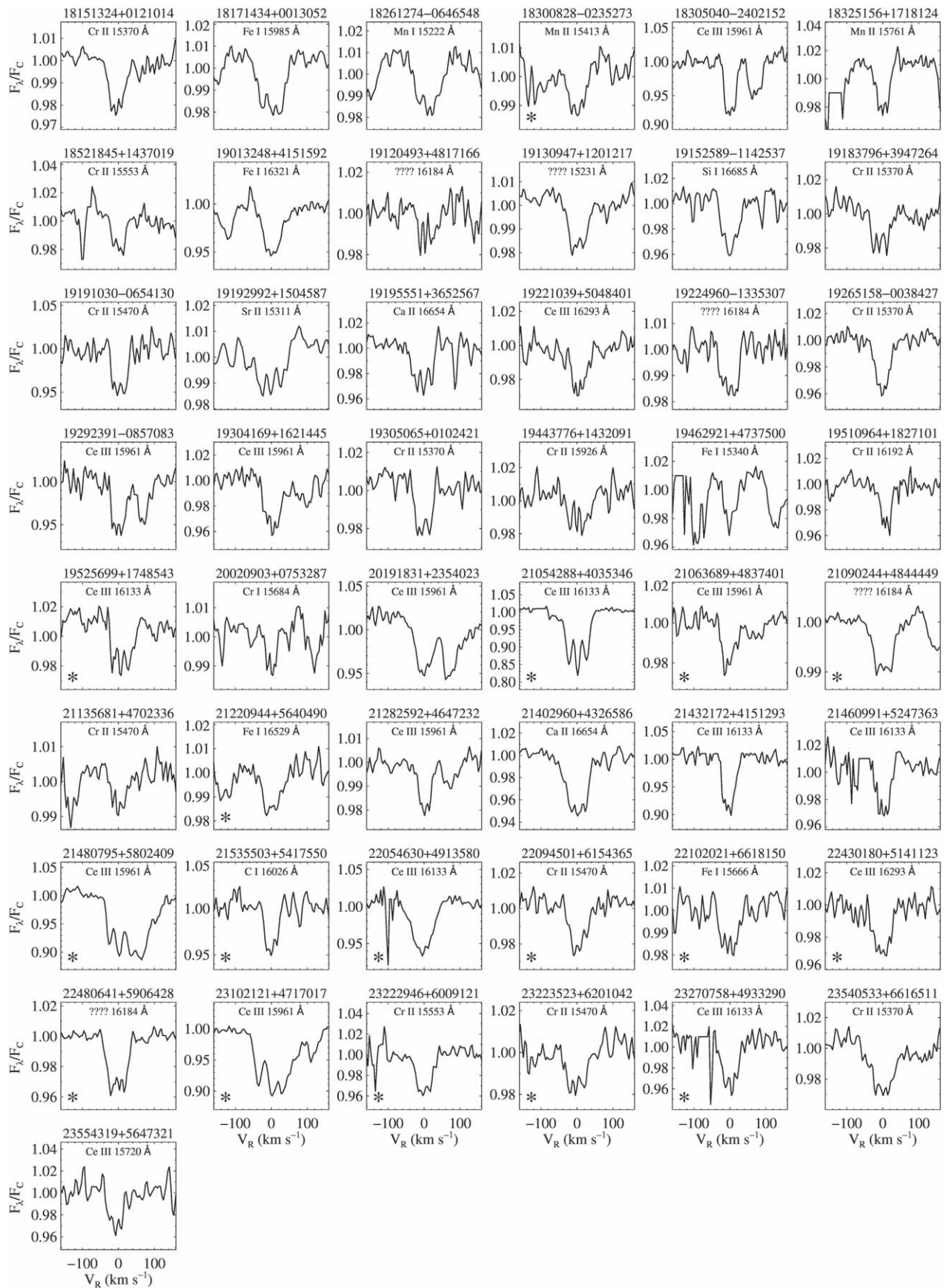
Figure 3. (Continued.)

Figure 3. (Continued.)

Table 2
Magnetic Field Modulus Estimates

2MASS ID	Other ID	V (mag)	H (mag)	N_{spectra}	S/N	Spec. Type	$\langle B \rangle$ (kG) H-band	N_{lines} H-band	$\langle B \rangle$ (kG) Optical	N_{lines} Optical
00033808+7018217	HD 225114	8.10	8.19	12	726	A0p SrCrSi[a]	7.46 ± 0.54	8	7.43 ± 0.32[a]	36
00102704+7337035	TYC 4306-1062-1	10.84	10.07	9	537	⋯	4.17 ± 0.28	16	⋯	⋯
00283062+6947472	TYC 4299-696-1	10.53	9.45	12	682	⋯	7.92 ± 0.89	4	⋯	⋯
00284036+8418313	TYC 4615-2915-1	10.96	10.54	14	332	A2V[b]	5.10 ± 0.22	17	⋯	⋯
00323366+5512530	HD 2887	9.79	8.17	13	1793	A2:p SrCr[a]	4.95 ± 0.24	25	4.97 ± 0.22[a]	27
00331847+5716167	TYC 3662-378-1	10.70	10.37	6	481	⋯	(8.53 ± 0.79)	5	⋯	⋯
00564145+5739255	TYC 3676-505-1	11.19	10.96	3	86	⋯	18.49 ± 0.76	6	⋯	⋯
00584870+6240562	TYC 4021-632-1	11.22	10.45	6	411	A2:p Eu[a]	4.25 ± 0.29	15	4.60 ± 0.19[a]	22
01052242+5010296	TYC 3271-1597-1	10.49	10.22	3	266	⋯	(6.79 ± 1.13)	3	⋯	⋯
01184266+5844433	TYC 3681-1528-1	10.49	9.99	4	355	B8[b]	9.67 ± 0.50	9	⋯	⋯

Notes.
[a] Own data (ARC 3.5 m/ARCES).
[b] Skiff (2014).
[c] Renson & Manfroid (2009).
[d] SIMBAD.
[e] Mathys (2017).
[f] Freyhammer et al. (2008).

(This table is available in its entirety in machine-readable form.)

6. Conclusions

Although spectroscopic observations at long wavelengths such as in the H-band help to maximize the $\Delta\lambda$ term of Equation (1) and to lessen the impact of blending due to the Doppler effect, this Letter represents the first serious exploitation of this wavelength regime for investigating the magnetic fields of Ap stars. The APOGEE sample of Ap stars with RMSLs represents a 183% increase in the number of Ap stars with $\langle B \rangle$ measurements, bringing the total to 238 stars. As the SDSS/APOGEE survey is still ongoing, this number is expected to increase. Detailed characterization of the now much larger sample of Ap stars with RSMLs may help to shed light on the origin of magnetic fields in stars with radiative envelopes as well as the relations between magnetism and other factors such as binarity and rotation. In particular, the investigation of the stellar parameters and chemical abundances of the sample would be a worthwhile effort, as would be high-resolution spectroscopic monitoring to measure the average value of $\langle B \rangle$ and the rotational period.

As demonstrated in the histogram of magnetic field modulus presented in Figure 2, more than 50% of Ap stars with magnetically split lines possess magnetic fields in the range of 4–7 kG. Despite the identification among the APOGEE sample of 19 new examples of stars with $\langle B \rangle > 10$ kG, led by 2MASS J02563098+4534239 ($\langle B \rangle = 25$ kG), the high-$\langle B \rangle$ tail of the distribution remains capped by the 34 kG magnetic field of Babcock's Star (HD 215441; Babcock 1960). The only other non-degenerate star known to approach 30 kG is HD 75049 (Elkin et al. 2010), for which $\langle B \rangle$ ranges from 24 to 30 kG over an orbital period. Among the more massive magnetic stars, which are He-rich early-type B stars, the strongest known magnetic field is only 21 kG (Hubrig et al. 2017). We can speculate that the magnetic field value of 34 kG likely represents a critical field strength above which stable magnetic fields do not exist in Ap stars. Such a limit would be probably be related to the restricted range of seed fields, of the order of milli-Gauss, that are observed in star-forming regions (Han & Zhang 2007).

ORCID iDs

S. Drew Chojnowski https://orcid.org/0000-0001-9984-0891

Swetlana Hubrig ⬤ https://orcid.org/0000-0003-0153-359X
David G. Whelan ⬤ https://orcid.org/0000-0002-6006-0537
Steven R. Majewski ⬤ https://orcid.org/0000-0003-2025-3147
Keivan G. Stassun ⬤ https://orcid.org/0000-0002-3481-9052

References

Babcock, H. W. 1960, ApJ, 132, 521
Biémont, E., Quinet, P., & Ryabchikova, T. A. 2002, MNRAS, 336, 1155
Blanton, M. R., Bershady, M. A., Abolfathi, B., et al. 2017, AJ, 154, 28
Castro, N., Fossati, L., Hubrig, S., et al. 2017, A&A, 597, L6
Chojnowski, S. D., Whelan, D. G., Wisniewski, J. P., et al. 2015, AJ, 149, 7
Eikenberry, S. S., Chojnowski, S. D., Wisniewski, J., et al. 2014, ApJL, 784, L30
Eisenstein, D. J., Weinberg, D. H., Agol, E., et al. 2011, AJ, 142, 72
Elkin, V. G., Mathys, G., Kurtz, D. W., Hubrig, S., & Freyhammer, L. M. 2010, MNRAS, 402, 1883
Freyhammer, L. M., Elkin, V. G., Kurtz, D. W., Mathys, G., & Martinez, P. 2008, MNRAS, 389, 441
Ghazaryan, S., Alecian, G., & Hakobyan, A. A. 2018, MNRAS, 480, 2953
Gray, R. O., & Corbally, C. J. 2009, Stellar Spectral Classification (Princeton, NJ: Princeton Univ. Press)
Gunn, J. E., Siegmund, W. A., Mannery, E. J., et al. 2006, AJ, 131, 2332
Han, J. L., & Zhang, J. S. 2007, A&A, 464, 609
Hubrig, S., Castelli, F., González, J. F., et al. 2012, A&A, 542, A31
Hubrig, S., Mikulášek, Z., Kholtygin, A. F., et al. 2017, MNRAS, 472, 400
Majewski, S. R., Schiavon, R. P., Frinchaboy, P. M., et al. 2017, AJ, 154, 94
Mathys, G. 1990, A&A, 236, 527
Mathys, G. 2017, A&A, 601, A14
Moss, D. 2001, in ASP Conf. Proc. 248, Magnetic Fields Across the Hertzsprung-Russell Diagram, ed. G. Mathys et al. (San Francisco, CA: ASP), 305
Nidever, D. L., Holtzman, J. A., Allende Prieto, C., et al. 2015, AJ, 150, 173
Preston, G. W. 1969, ApJ, 156, 967
Prugniel, P., & Soubiran, C. 2001, A&A, 369, 1048
Renson, P., & Manfroid, J. 2009, A&A, 498, 961
Shetrone, M., Bizyaev, D., Lawler, J. E., et al. 2015, ApJS, 221, 24
Skiff, B. A. 2014, yCat, 2023, 1
Skrutskie, M. F., Cutri, R. M., Stiening, R., et al. 2006, AJ, 131, 1163
Wang, S.-i., Hildebrand, R. H., Hobbs, L. M., et al. 2003, Proc. SPIE, 4841, 1145
Zacharias, N., Finch, C. T., Girard, T. M., et al. 2013, AJ, 145, 44
Zasowski, G., Cohen, R. E., Chojnowski, S. D., et al. 2017, AJ, 154, 198
Zasowski, G., Johnson, J. A., Frinchaboy, P. M., et al. 2013, AJ, 146, 81

Erratum: "Discovery of Resolved Magnetically Split Lines in SDSS/APOGEE Spectra of 157 Ap/Bp Stars" (2019, ApJL, 873, L5)

S. Drew Chojnowski[1] , Swetlana Hubrig[2] , Sten Hasselquist[3], Fiorella Castelli[4], David G. Whelan[5] , Steven R. Majewski[6] , Christian Nitschelm[7], D. A. García-Hernández[8,9], Keivan G. Stassun[10] , and Olga Zamora[8,9]

[1] Apache Point Observatory and New Mexico State University, P.O. Box 59, Sunspot, NM 88349-0059, USA
[2] Leibniz-Institut für Astrophysik Potsdam (AIP), An der Sternwarte 16, D-14482 Potsdam, Germany
[3] Department of Physics & Astronomy, University of Utah, 115 1400 E, Salt Lake City, UT 84112, USA
[4] Istituto Nazionale di Astrofisica, Osservatorio Astronomico di Trieste, via Tiepolo 11, I-34143 Trieste, Italy
[5] Department of Physics, Austin College, 900 N. Grand Ave., Sherman, TX 75090, USA
[6] Department of Astronomy, University of Virginia, P.O. Box 400325, Charlottesville, VA 22904-4325, USA
[7] Centro de Astronomía (CITEVA), Universidad de Antofagasta, Avenidos Angamos 601, Antofagasta 1270300, Chile
[8] Instituto de Astrofísica de Canarias (IAC), E-38205 La Laguna, Tenerife, Spain
[9] Universidad de La Laguna (ULL), Departamento de Astrofísica, E-38206 La Laguna, Tenerife, Spain
[10] Department of Physics and Astronomy, Vanderbilt University, Nashville, TN 37235, USA

Supporting material: machine-readable table

In the online-only version of Table 1, effective Landé g Factors, the Si I and Si II lines were mislabeled as S II and S III, even though the associated atomic data pertains to neutral and singly ionized Silicon. We apologize for any confusion caused by the error, and we thank Alexander Kramida for pointing it out.

Table 1
Effective Landé g Factors

Ion	λ_{vac} (Å)	log(gf)	J_{low}	g_{low}	E_{low} (eV)	J_{high}	g_{high}	E_{high} (eV)	g_{eff}	N_{stars}
C I	16009.273	−0.090	2.0	1.000	9.631	3.0	1.001	10.406	1.002 ± 0.050	3
C I	16026.078	−0.140	2.0	1.000	9.631	3.0	1.074	10.405	1.148 ± 0.050	6
C I	16895.031	0.568	2.0	1.000	9.003	3.0	0.978	9.736	0.956 ± 0.050	19
Mg I	15753.291	−0.060	1.0	1.501	5.932	2.0	1.167	6.719	1.000 ± 0.050	2
Mg I	15770.150	0.380	2.0	1.501	5.933	3.0	1.334	6.719	1.167 ± 0.050	8

(This table is available in its entirety in machine-readable form.)

ORCID iDs

S. Drew Chojnowski https://orcid.org/0000-0001-9984-0891
Swetlana Hubrig https://orcid.org/0000-0003-0153-359X
David G. Whelan https://orcid.org/0000-0002-6006-0537
Steven R. Majewski https://orcid.org/0000-0003-2025-3147
Keivan G. Stassun https://orcid.org/0000-0002-3481-9052